Supporting information

Potential Well Effect for Efficient Oxygen Reduction and Corrosion Resistance under Operating Temperature Conditions of PEMFCs

Chang Li[a,b] ,Yiyang Mao[a], Ji Qiu[b], Xixi Wang[a], Jie Miao[c], Yulin Min[b]*, Wei Zhou[a,d]* and Zongping Shao[e]*

[a]*State Key Laboratory of Materials-Oriented Chemical Engineering, College of Chemical Engineering, Nanjing Tech University, Nanjing, 211816, China*

[b]*Shanghai Key Laboratory of Materials Protection and Advanced Materials Electric Power, Shanghai Engineering Research Center of Energy-Saving in Heat Exchange Systems, Shanghai University of Electric Power, Shanghai 200090, P. R. China.*

[c]*Collge of Environmental Science and Engineering, Nanjing Tech University, Nanjing 211816, China.*

[d]*Suzhou Laboratory, Suzhou 215000, China.*

[e]*Department of Chemical Engineering, Curtin University, Perth, 6845, Australia*

Corresponding Author:

*E-mail: minyulin@shiep.edu.cn (Y.M.)

*E-mail: zhouwei1982@njtech.edu.cn (W.Z.)

*E-mail: zongping.shao@curtin.edu.au (Z.S.)

Experimental section

Chemicals and Materials

Zinc nitrate hexahydrate ($Zn(NO_3)_2 \cdot 6H_2O$), chloroplatinic acid hexahydrate ($H_2PtCl_6 \cdot 6H_2O$), polyvinylidene fluoride (PVDF), ethanol (AR), isopropanol (AR) perchloric acid (AR),and sulfuric acid (AR) were purchased from Aladdin. Commercial carbon nanotubes (CNTs) were obtained from Xianfeng Nanomaterials Technology Co., Ltd. Commercial 20 wt.%Pt/C was obtained from Shanghai Hesen Electrical Co., Ltd. All chemicals were used without further purification. The deionized water used in electrochemical measurements was ultrapure (18.2 MΩ cm)

Synthesis of F-CNT

F-CNT is obtained by acid etching of CNT and high-temperature calcination of F source. First, 2.0 g of carbon nanotubes are uniformly dispersed in 100 ml of HNO_3 through ultrasound for 1 h, and then refluxed in a 150 ℃ oil bath for 3 h. The resulting sample is centrifuged (10000 rpm), then washed with pure water, centrifuged again, until the pH of the sample reaches ~7. The obtained acid-etched CNT with a large number of defects and oxygen-containing groups (denoted as O-CNT) is dried at 80 °C overnight. Subsequently, 0.2 g O-CNT and 1.0 g PVDF are mixed in an agate mortar and ground for 1 h, followed by thermal decomposition at 700 °C in an Ar atmosphere for 2 h, with a heating rate of 5 ℃ min^{-1}. After cooling to room temperature, F-CNT is obtained.

Synthesis of Electrocatalysts

The water solution containing $H_2PtCl_6 \cdot 6H_2O$ and $Zn(NO_3)_2 \cdot 6H_2O$ was traditionally impregnated, and then high-temperature thermal reduction in 5% H_2/Ar was used to prepare PtZn i-NPs/F-CNT. Typically, $H_2PtCl_6 \cdot 6H_2O$ and $Zn(NO_3)_2 \cdot 6H_2O$, along with 50 mg of F-CNT carrier, were mixed in a 100 ml round-bottom flask with 50 mL of deionized water. The total metal content was controlled at 20 wt% under a Pt-to-Zn molar ratio of 1:1. After stirring the mixture overnight, it was frozen in a refrigerator overnight and then freeze-dried to obtain the dried precursor. Finally, the dried powder was subjected to high-temperature reduction at 800 °C for 2 hours in a 5% H_2/Ar

atmosphere. Pt NPs supported on F-CNT and PtZn NPs supported on CNT were prepared using the same procedure.

Structural Characterization

The contents of Pt and Zn in PtZn i-NPs/F-CNT, PtZn/CNT were determined by inductively coupled plasma atomic emission spectrometry (ICP-OES, Agilent ICPOES730) and CHNSO element analyzer (Analytic Jena EA3000). X-ray diffraction (XRD) was performed on the Bruker AXS D8 Advance X-ray diffractometer, Cu Kα Radiation at 40 KV and 40 mA, 2θ angle starts at 10 ° and ends at 90 °. High resolution transmission electron microscopy (HRTEM) and element mapping were performed on the FEI TALOS F200 at an accelerating voltage of 200 KV. The surface state analysis of each element uses monochromated Al Ka through XPS α Source (hν = 1486.6 eV) on the Thermo ESCALAB 250xi system, the power is 150 W, and the passing energy is 30 eV. Horiba Jobin Yvon Lab RAM spectra were collected under 532 nm laser excitation using a 100x objective lens.

Electrochemical infrared spectroscopy.

Attenuated total reflection surface-enhanced infrared absorption measurements were performed on a homemade spectro-electrochemical cell. The catalyst was drop-casted on a ~60-nm-thick SEIRA-active Au film, which was pre-deposited on the reflection plane of a semicircular cylinder Si prism. Electrochemical ATR–SEIRAS measurements were then performed in an optical system embedded in the spectroscopic chamber. Spectra are shown as absorbance, defined as $A = -\log I_1 / I_2$, where I_1 and I_2 represent the irradiation intensity of incident and reflective beams, respectively.

Electrochemical properties of catalysts

A mixture of 2 mg catalyst, 400 μl isopropanol, 20 μl 5 wt% Nafion solution, and 600 μl deionized water was prepared and sonicated for 30 min to prepare the catalyst ink. 10 μl of the catalyst ink was dropped onto the glassy carbon surface of the rotating disk electrode (RDE, 5mm in diameter, Pine Instruments), and then dried at room temperature. Unless otherwise stated, Pt/C (20 wt%) was fixed at ~20 μg cm^{-2}.

Electrochemical tests were performed on a CHI-760 electrochemical workstation. The working electrode was equipped with an RDE system (Pine Research Instruments).

Experiments were carried out at 25 °C with a reversible hydrogen electrode (RHE) as reference electrode and a carbon rod as the counter electrode. The cyclic voltammetry of the catalysts was measured in Ar-saturated 0.1 M HClO4. The potential range of the CV was 0.05- 1.05 V versus RHE (scan rate 50 mV s^{-1}). The oxygen reduction reaction (ORR) polarization curve was measured in O_2-saturated 0.1 M $HClO_4$ with the RDE rotating at 1600 rpm. Accelerated durability tests (ADTs) of the catalysts were performed by cycling the potential between 0.6 and 1.0 V vs. RHE (scan rate of 100 mV s^{-1} at 25 °C) in O_2-saturated 0.1 M $HClO_4$. All linear scanning voltametric curves were IR corrected. In calculating the mass activity, electrochemical surface area and specific activity during durability testing, the Pt loading on the initial working electrode is used.

Membrane Electrode Assembly (MEA) preparation

In this study, 4 cm^2 active area MEAs were generated using the standard CCM preparation procedure. The cathode catalyst inks were made by combining catalyst powders with a 5% Nafion® emulsion (DuPont de Nemours) and isopropyl alcohol, with an ionomer to carbon ratio of 0.4:1. Using an ultrasonic spraying machine (Siansonic UC320), the PtZn i-NPs/F-CNT catalyst was uniformly sprayed on one side of the Nafion® NR211 (DuPont de Nemours) at 75°C to obtain a Pt loading of 0.1 mg cm^{-2}. The other side of the membrane was sprayed with JM Pt/C, yielding an anode with a Pt loading of 0.05 mg cm^{-2}. Carbon paper with a gas diffusion layer was then used for hot pressing (2 Mpa) at 110 °C. At a test temperature of 80 °C and a back pressure of 1.5 bar, air (1000 sccm) and hydrogen (300 sccm) were fed to the cathode and anode, respectively, during the H_2-Air fuel cell test. At 80 °C, Air was supplied via the cathode, and the AST featured repetitive triangle wave cycling between 0.6 V to 0.9 V, with a sweep speed of 100 mV s^{-1}. The fast triangular wave potential cycling to accelerate the corrosion of the carbon carrier itself (electrochemical window: 1.0V-1.5V, atmosphere: H2/N2, cycling time: 2s). The MEA's operating voltage of 0.67 V was used for the constant voltage stability test.

DFT calculations

Density functional theory (DFT) calculations were conducted via Vienna Ab-initio

Simulation Package (VASP) software package. The projector-augmented wave (PAW) methodology and the generalized gradient approximation (GGA) within Perdew–Burke–Ernzerhof (PBE) were selected to perform the electronic structure calculations (Comp. Mater. Sci. 6 (1) (1996) 15-50.; Phys. Rev. Lett. 77 (18) (1996) 3865-3868.). The cut-off energy was set to 450 eV, while the K-points were set to 3 × 3 × 1 for density of states calculation and for others. Atomic structures were fully relaxed until the force on each atom was 0.05eV $Å^{-1}$. To ensure that the calculation results are reasonable, dispersion-corrected DFT-D3 method was set for absorption models. The calculation data were analyzed by vaspkit Code.

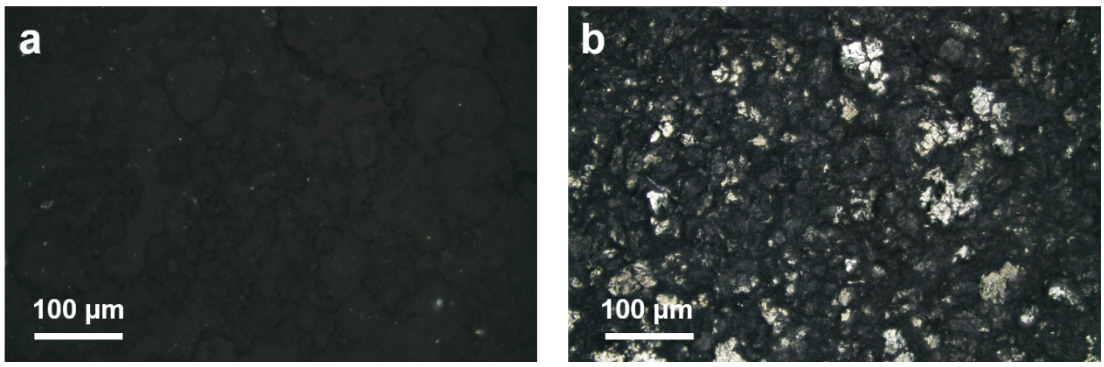

Figure S1. metallographic microscope images of a) PtZn i-NPs/F-CNT and b) PtZn/CNT

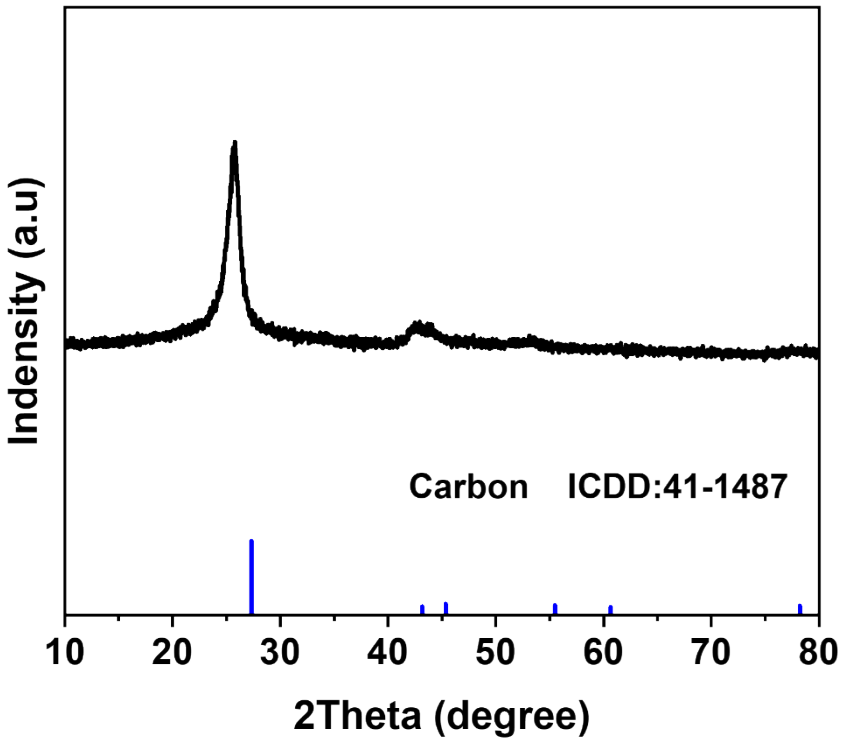

Figure S2.XRD of CNT

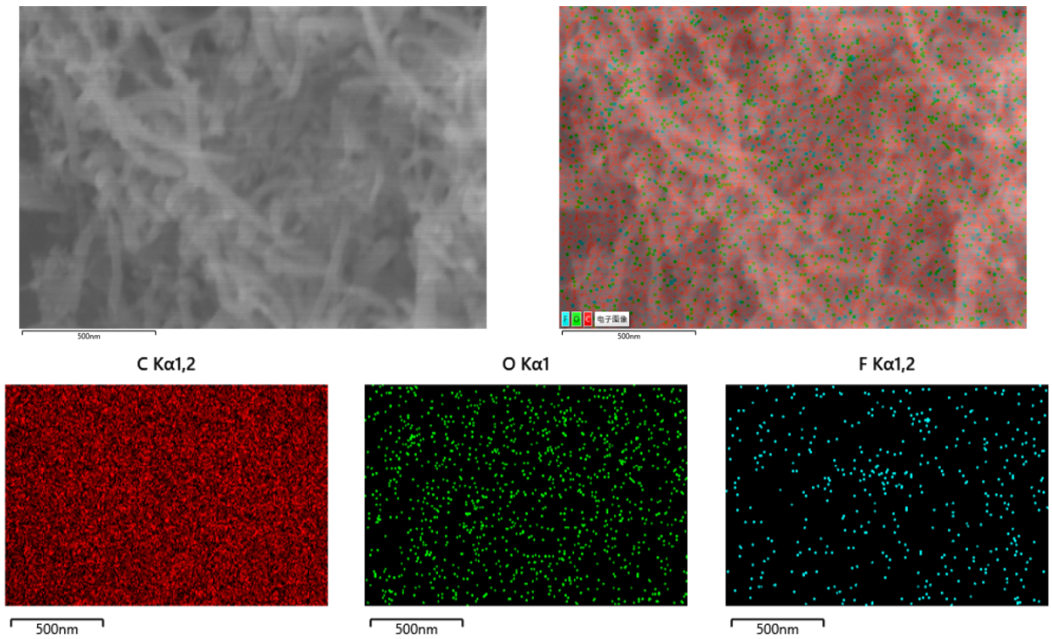

Figure S3.EDS of F-CNT

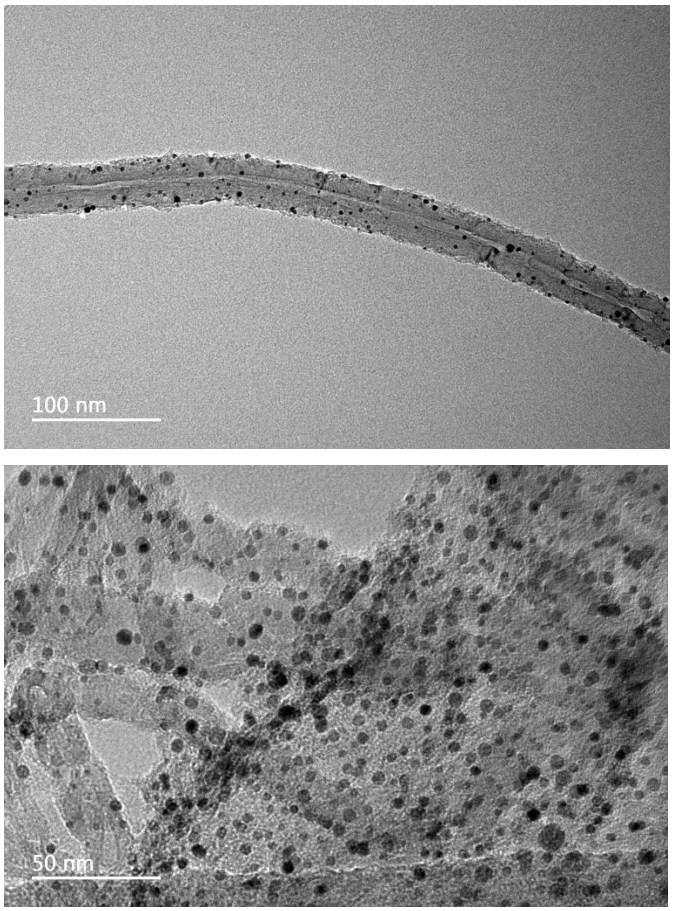

Figure S4. TEM of PtZn i-NPs/F-CNT

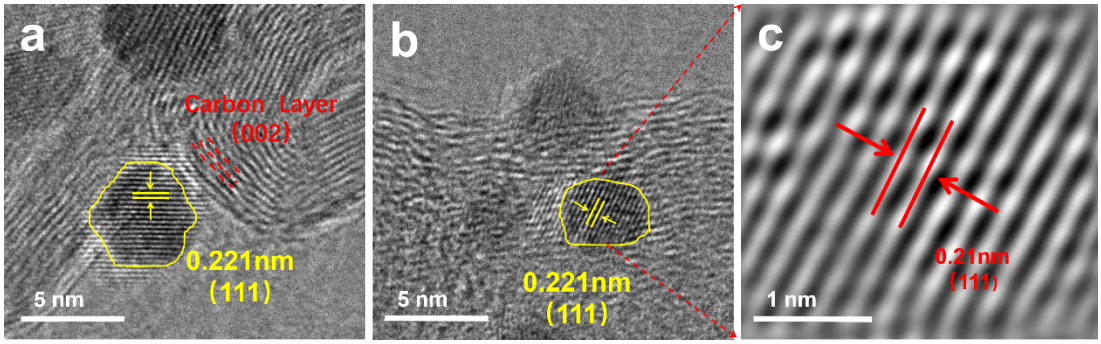

Figure S5. HRTEM of PtZn i-NPs/F-CNT

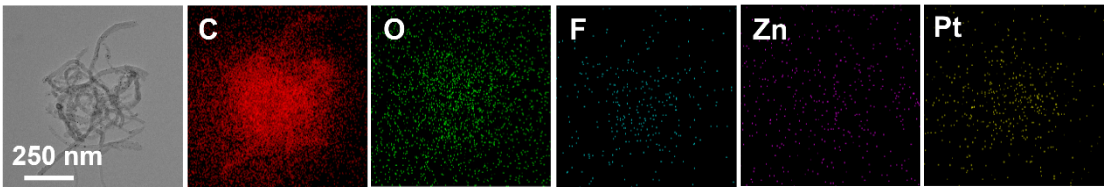

Figure S6. EDS of PtZn/F-CNT

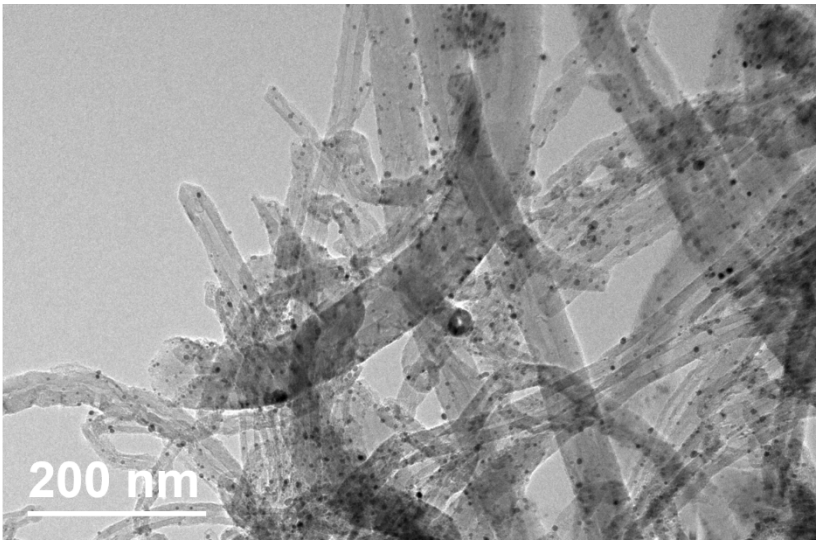

Figure S7. TEM of Pt /F-CNT

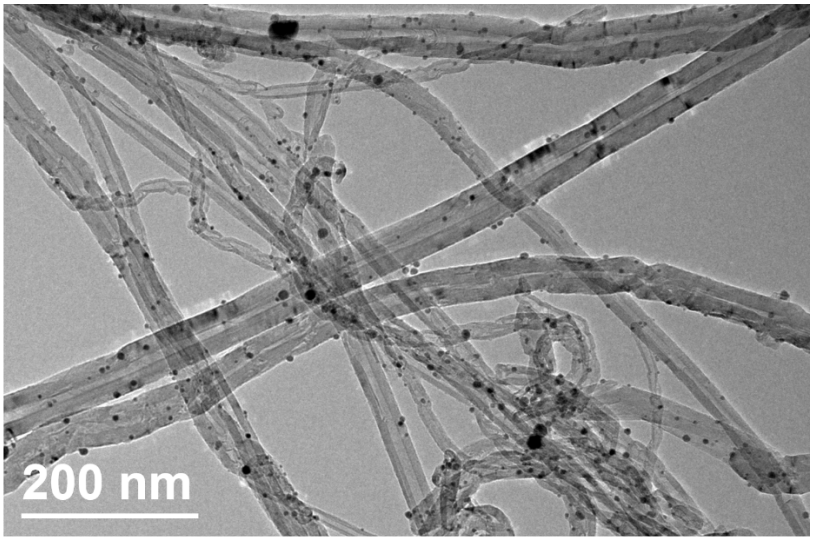

Figure S8. Pt /CNT

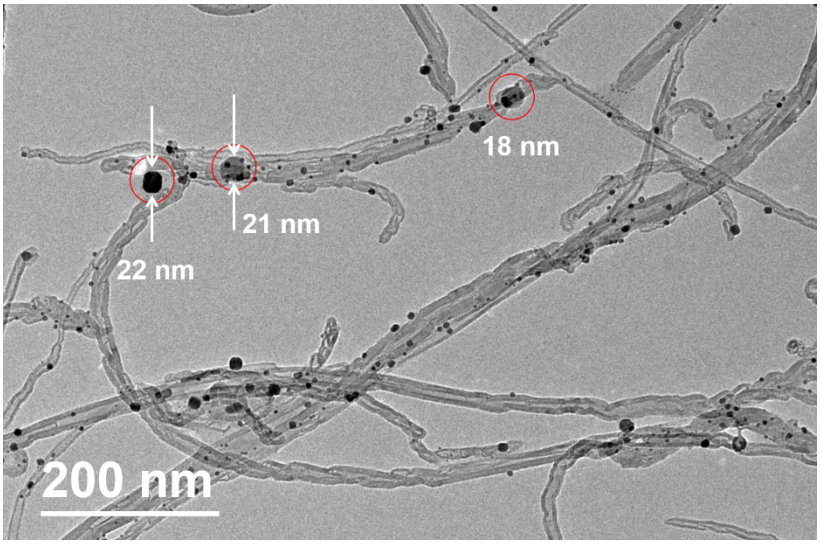

Figure S9. TEM of PtZn/CNT

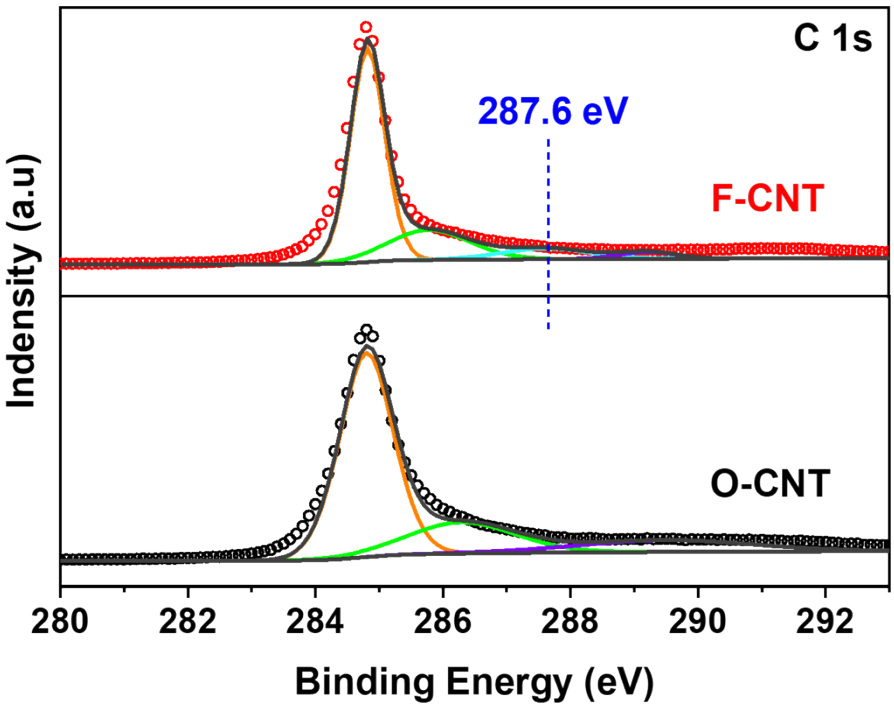

Figure S10. XPS of C1s

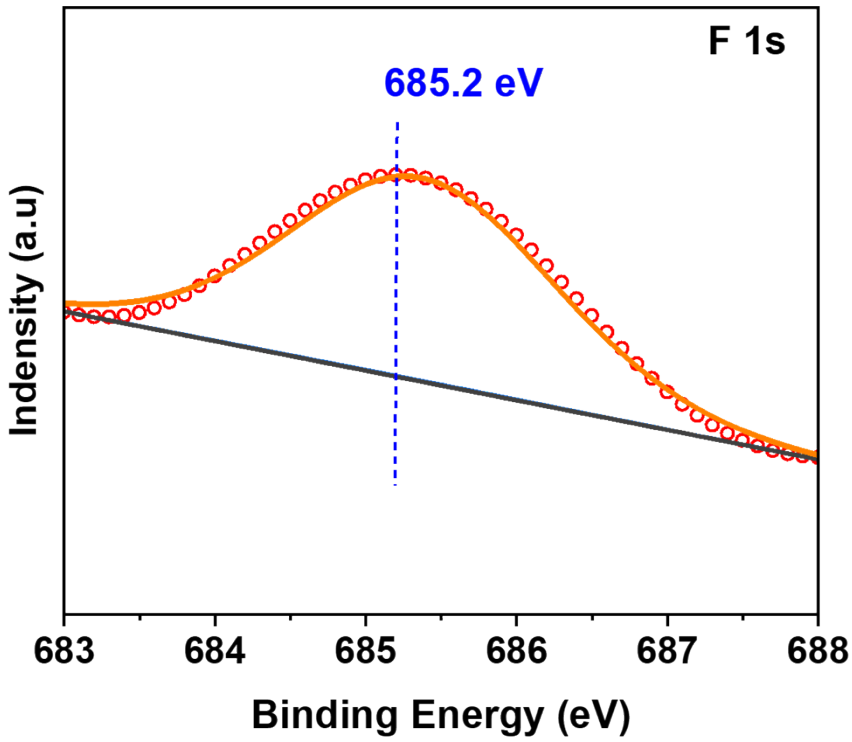

Figure S11. XPS of C1s

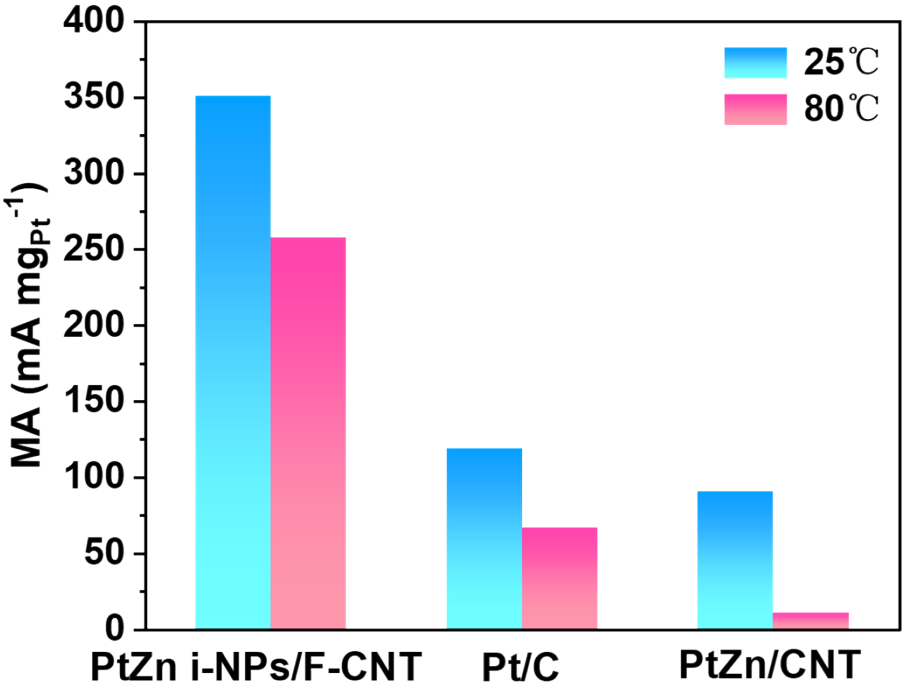

Figure S12. MA of PtZn i-NPs/F-CNT,Pt/C and PtZn/CNT

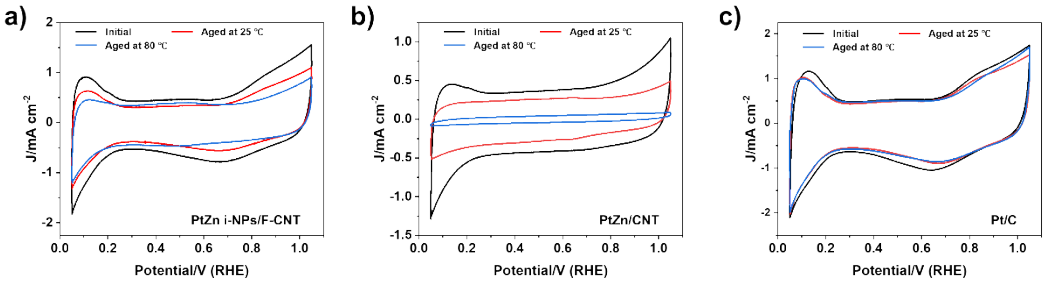

Figure S13. CV curves of in an N_2-saturated 0.1M $HClO_4$ solution at different temperature after ADT, with a scan rate of ~50 mV/s.

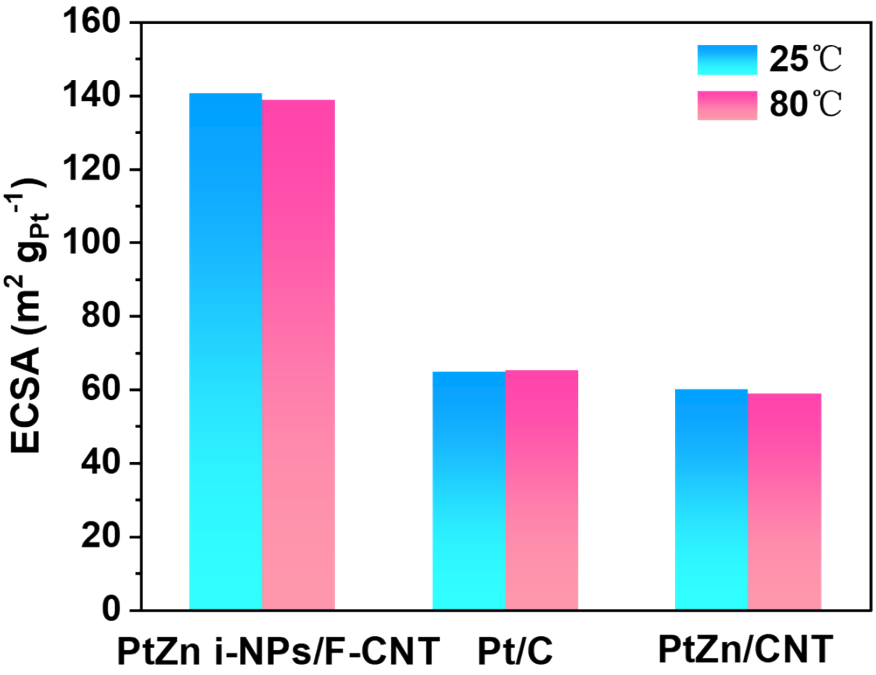

Figure S14. ECSA of PtZn i-NPs/F-CNT,Pt/C and PtZn/CNT

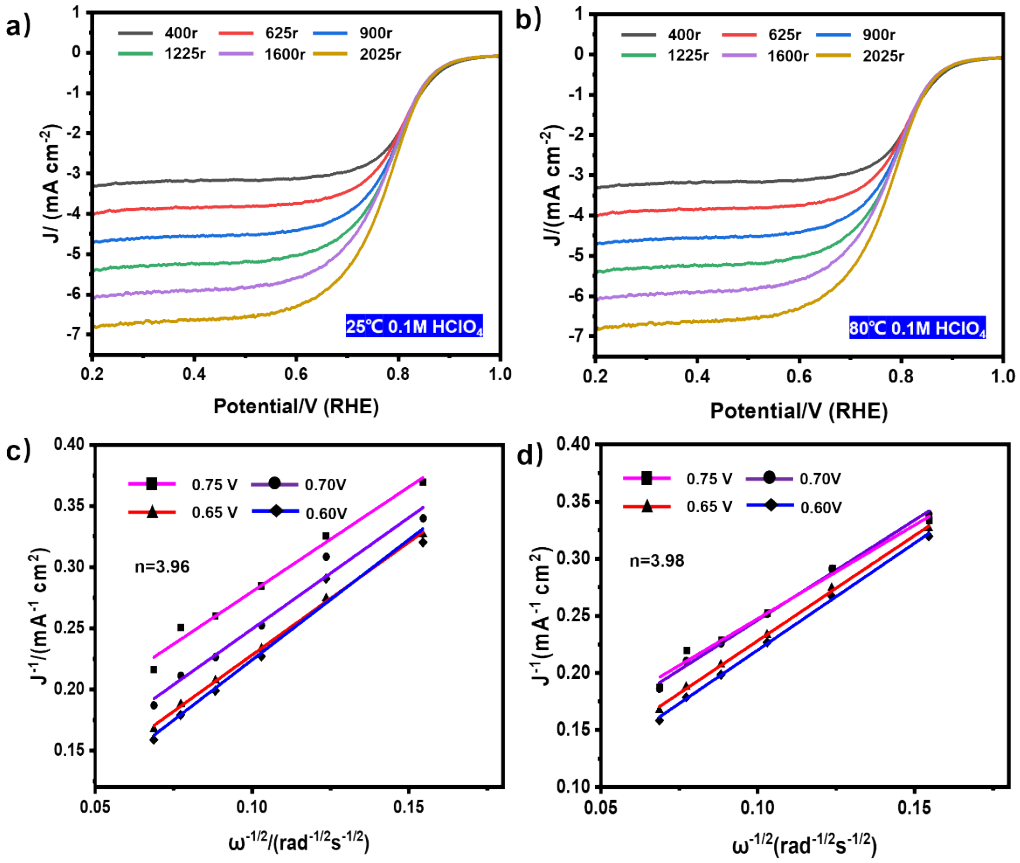

Figure S15.ORR performance of PtZn i-NPs/F-CNT at 80 °C. (a) LSVs at various rotating speeds. (b) Electron transfer number

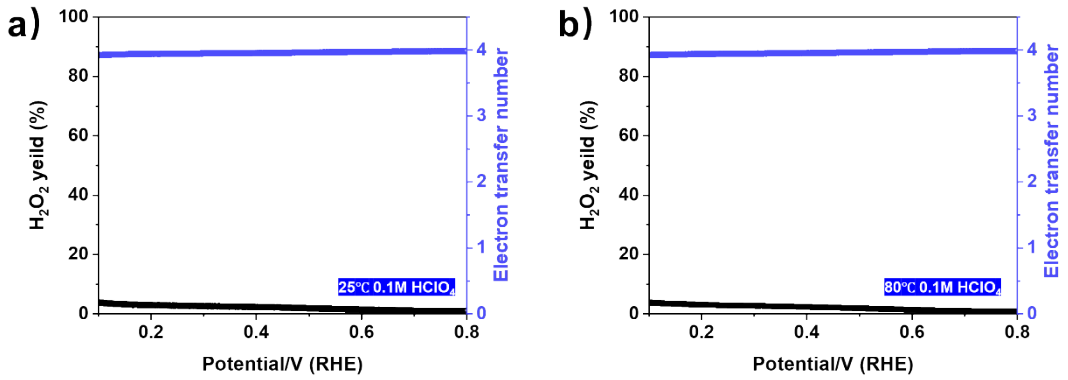

Figure S16. the H_2O_2 yeild and electron transfer number of PtZn i-NPs/CNT: (a) 25 ℃; (d) 80 ℃.

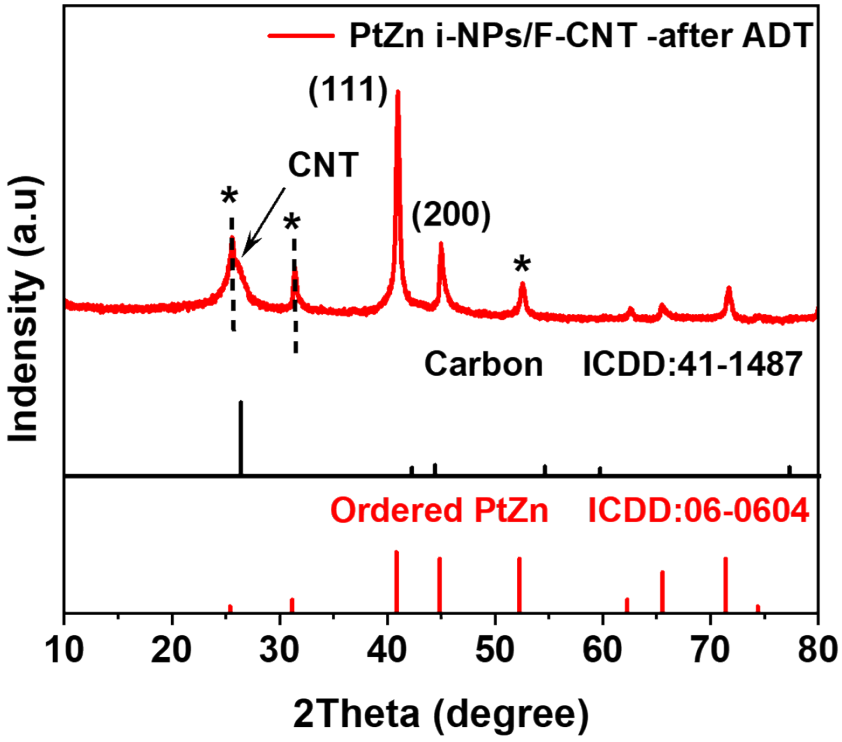

Figure S17. XRD of PtZn i-NPs/F-CNT after ADT

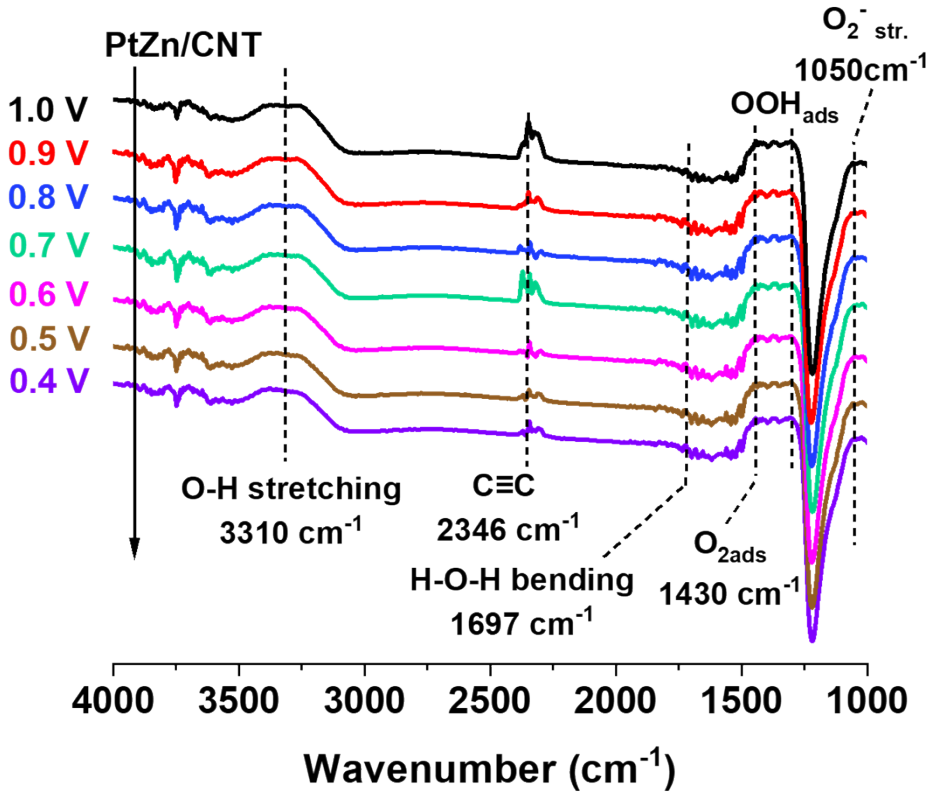

Figure S18. In-situ Fourier Transform infrared (FTIR) spectroscopy of voltage changes for PtZn/CNT

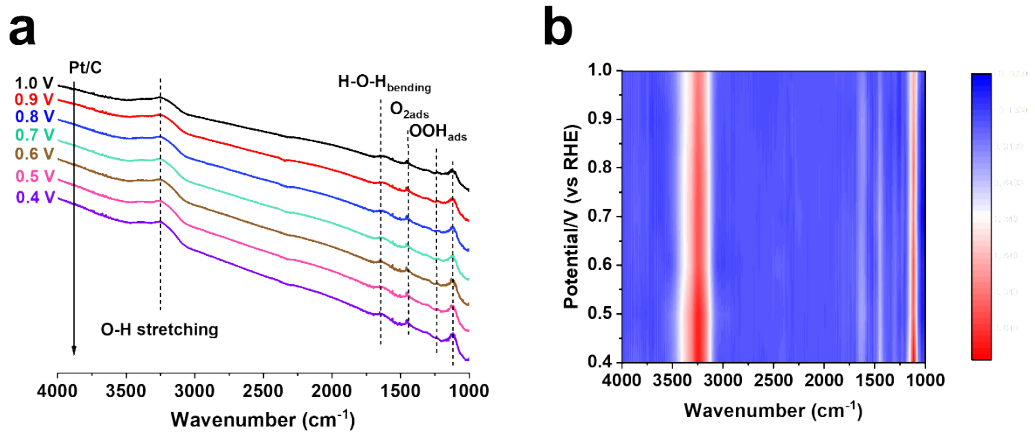

Figure S19. In-situ Fourier Transform infrared (FTIR) spectroscopy of voltage changes for Pt/C

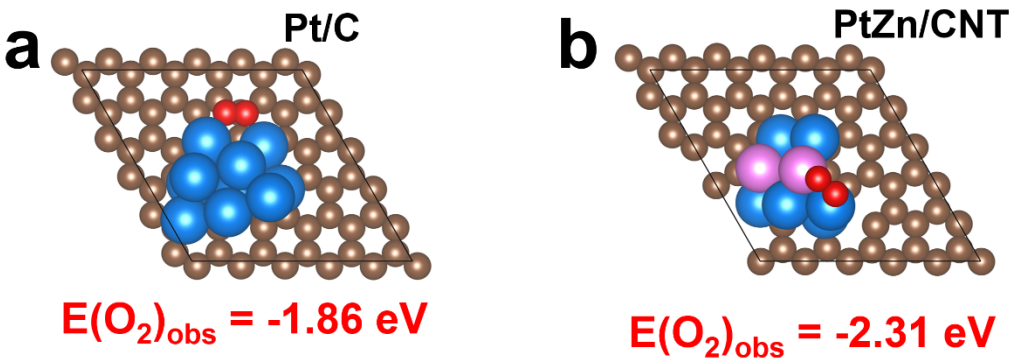

Figure S20. (a) oxygen adsorption of Pt/C; (b) oxygen adsorption of PtZn/CNT

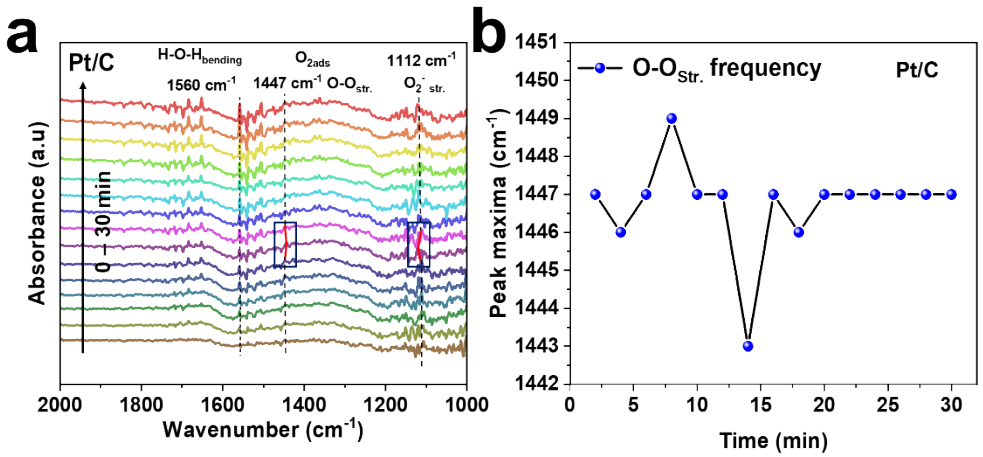

Figure S21. In-situ Fourier Transform infrared (FTIR) spectroscopy of time changes for Pt/C

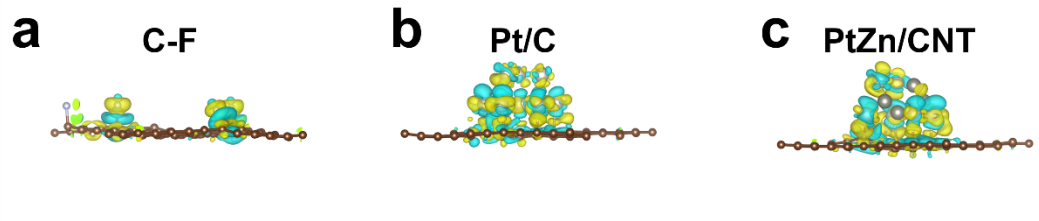

Figure S22. The differential charge density maps of C-F, Pt/C, PtZn/CNT

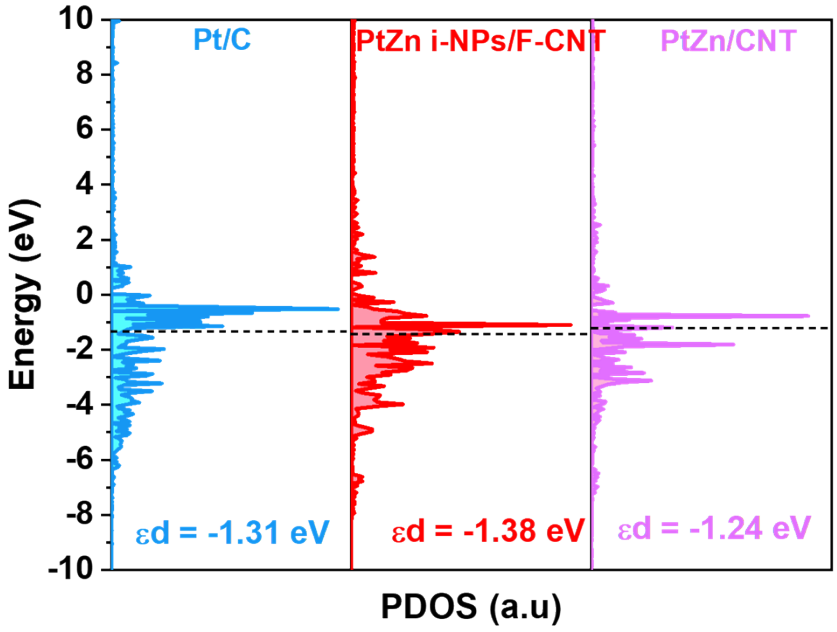

Figure S23. The PDOS of Pt/C, PtZn i-NPs/F-CNT and PtZn/CNT

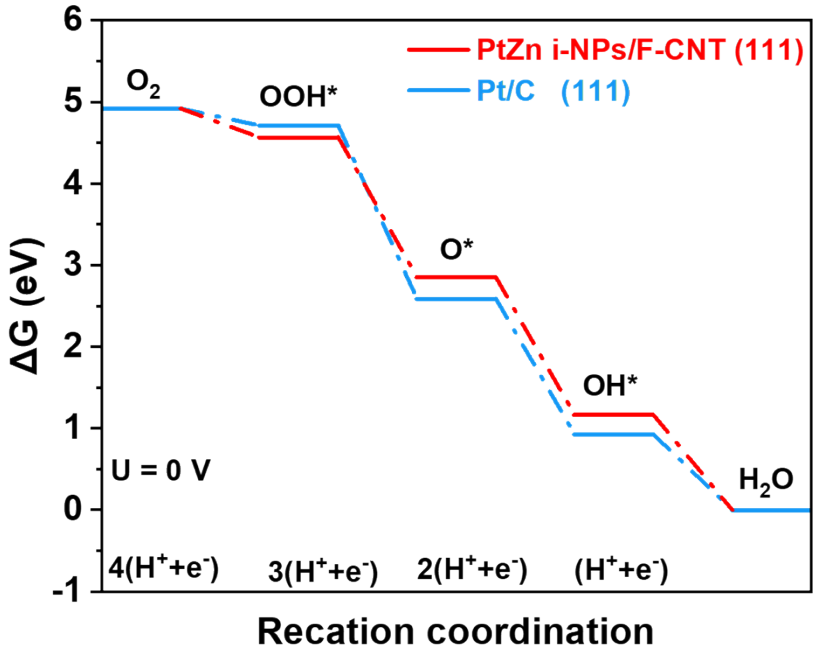

Figure S24. Calculated free energy diagrams for ORR on the PtZn i-NPs/F-CNT surface and Pt/C surface at 0V.

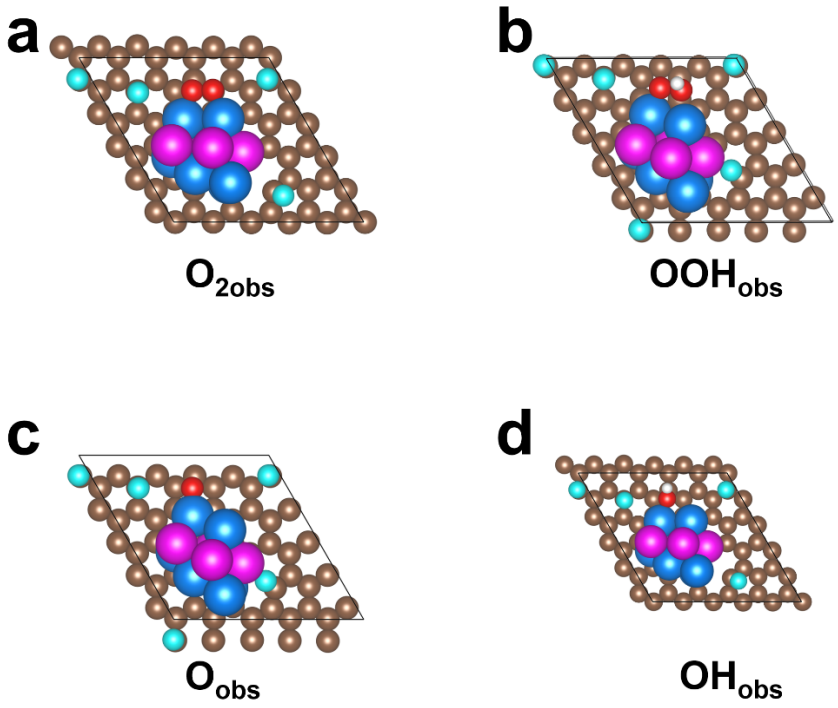

Figure S25. Four intermediate state models of ORR on the PtZn i-NPs/F-CNT surface.

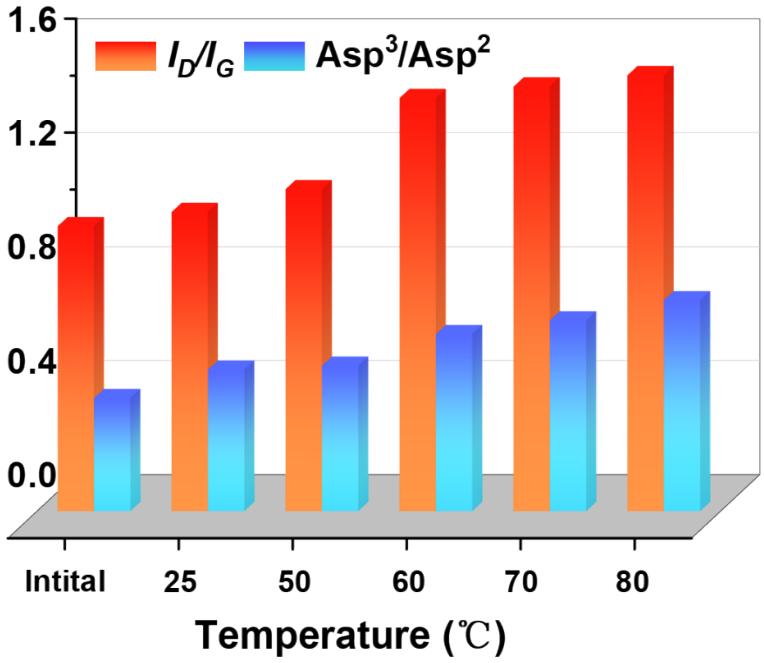

Figure S26. The I_D/I_G ratio and Asp^3/Asp^2 of Pt/C after ADT at different temperatures.

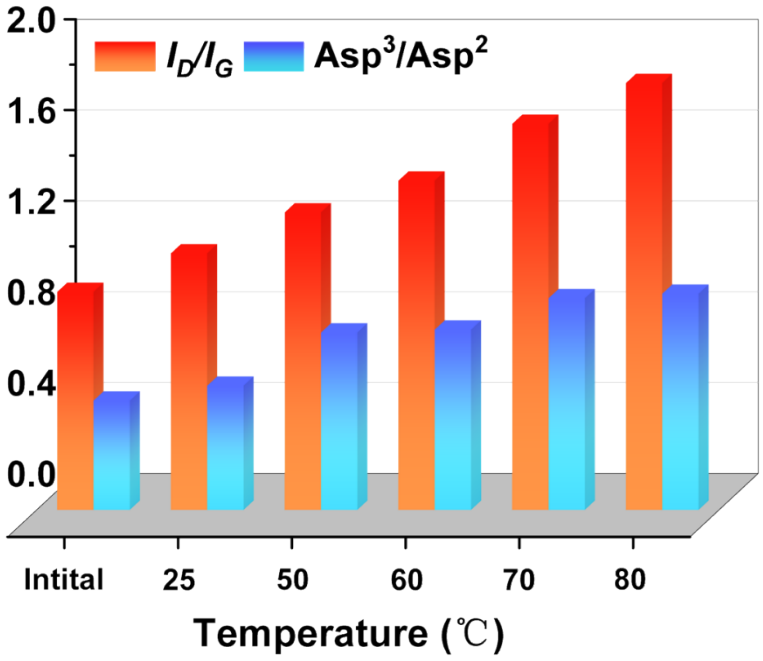

Figure S27. The I_D/I_G ratio and Asp^3/Asp^2 of PtZn/CNT after ADT at different temperatures.

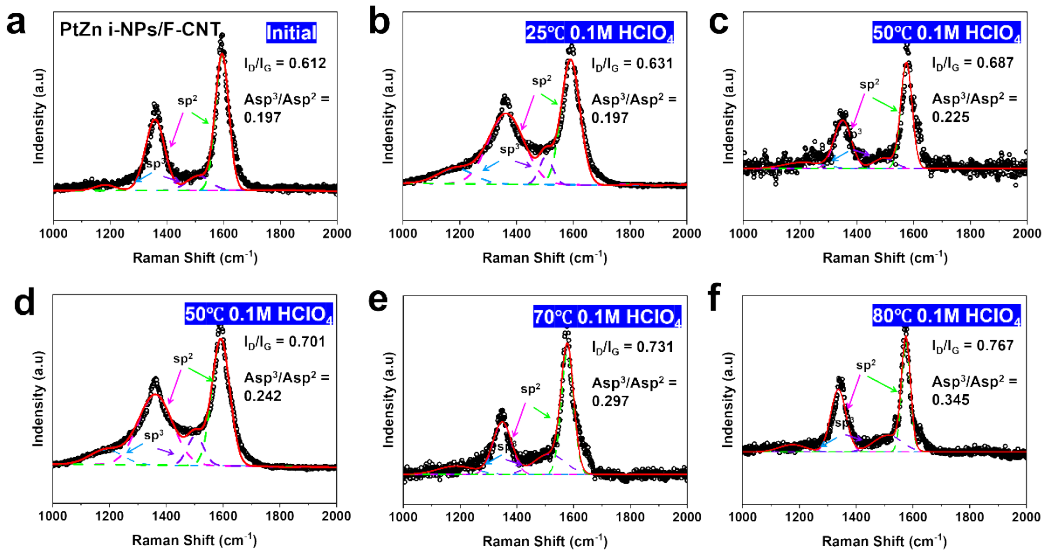

Figure S28. the Raman spectrum of PtZn i-NPs/F-CNT after ADT at different temperature

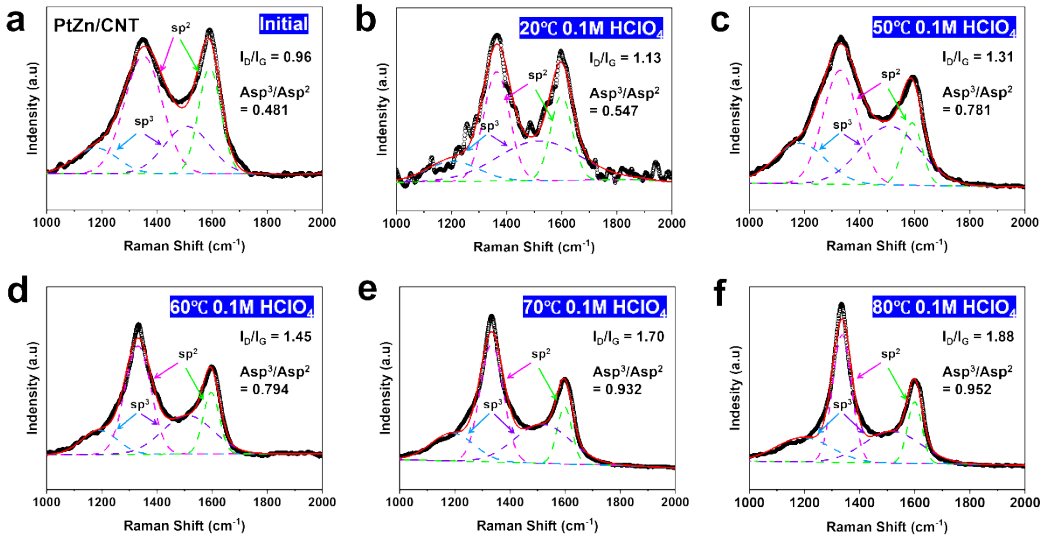

Figure S29. the Raman spectrum of PtZn/CNT after ADT at different temperature

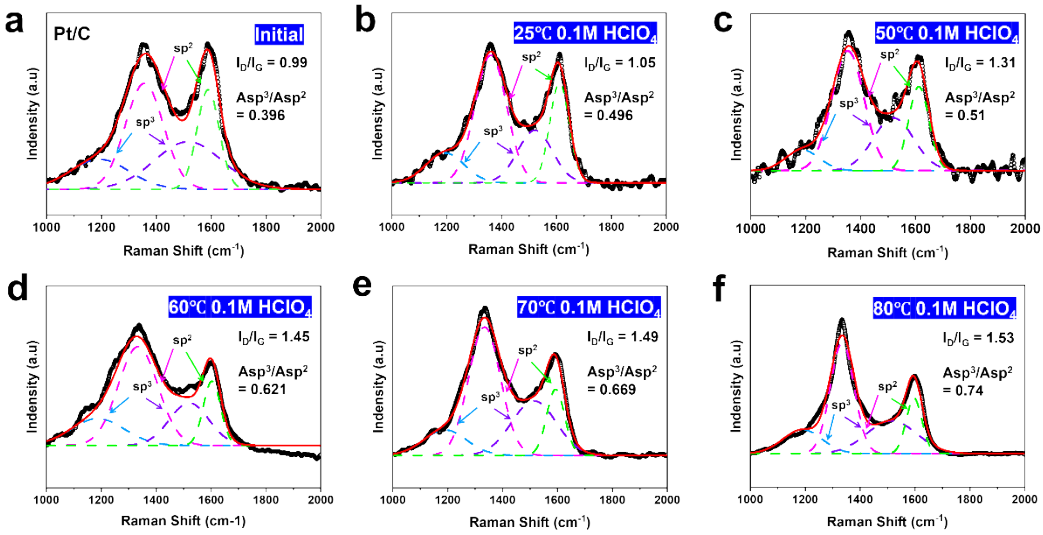

Figure S30. the Raman spectrum of Pt/C after ADT at different temperature

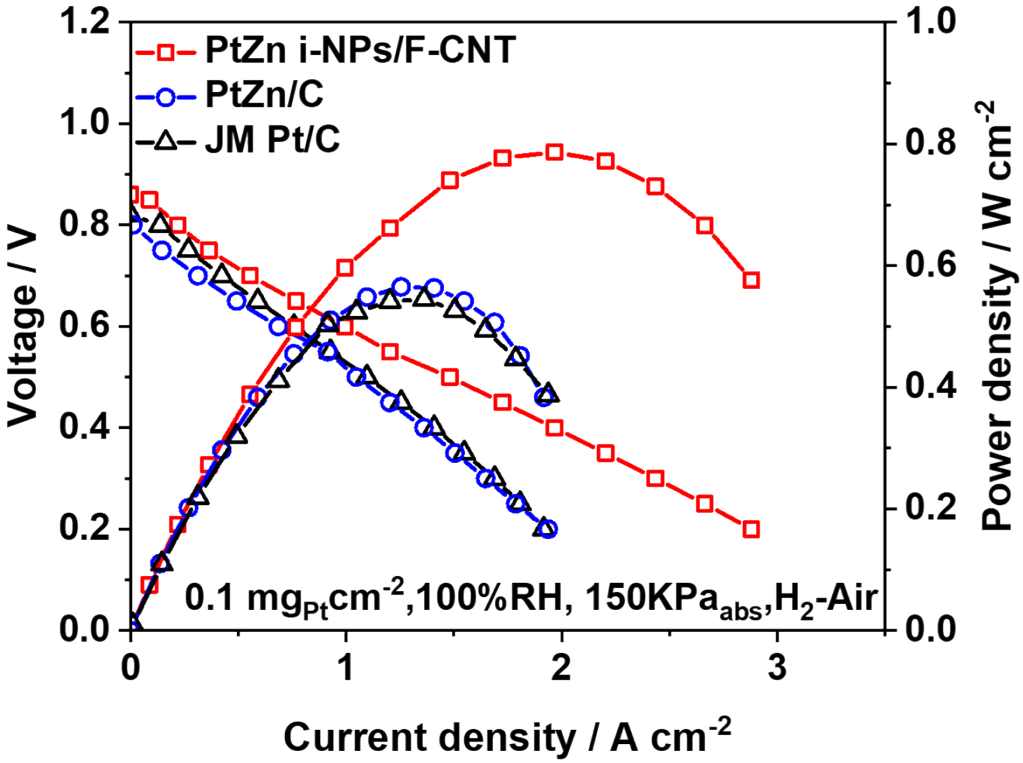

Figure S31. H_2-Air fuel cell polarization and i-P curves

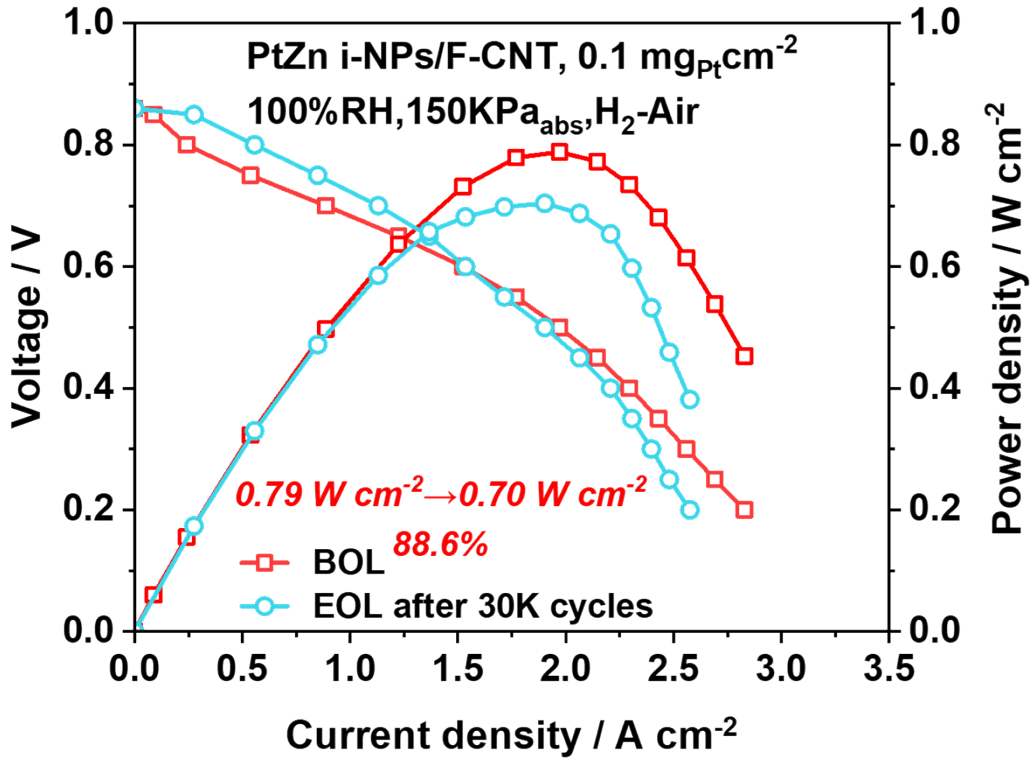

Figure S32. H_2-Air fuel cell polarization and i-P curves of PtZn i-NPs/F-CNT after 30K cycles AST. Cathode:0 1 mg_{Pt} cm^{-2}; Anode: 0.05 mg_{Pt} cm^{-2}; Total precious metal loading of MEA: 0.15 mg_{Pt} cm^{-2}

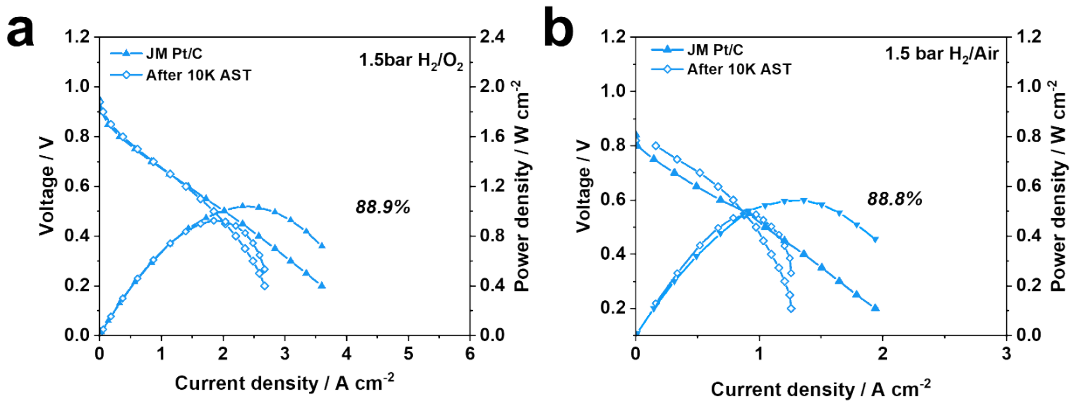

Figure S33. H_2-O_2 and H_2-Air fuel cell polarization and i-P curves of Pt/C after 10 000 AST. Cathode:0 1 mg_{Pt} cm^{-2}; Anode: 0.05 mg_{Pt} cm^{-2}; Total precious metal loading of MEA: 0.15 mg_{Pt} cm^{-2}

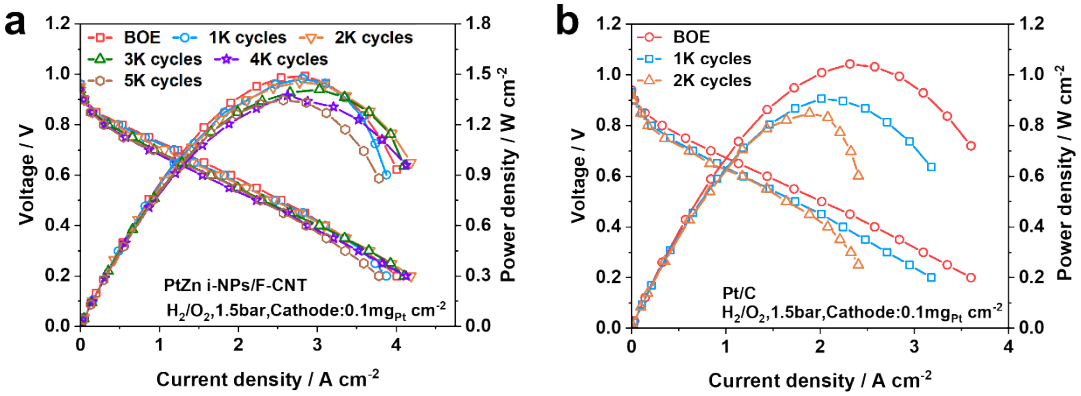

Figure S34. H_2-O_2 fuel cell polarization and i-P curves of PtZn i-NPs/F-CNT and Pt/C after testing. (a) PtZn i-NPs/F-CNT; (b) Pt/C. Cathode:0 1 mg_{Pt} cm^{-2}; Anode: 0.05 mg_{Pt} cm^{-2}; Total precious metal loading of MEA: 0.15 mg_{Pt} cm^{-2}.

Table S1 Table for spectral lines and corresponding electronic states, peak positions.

Sample name	Elements	Peak position (eV)	Spectral line	Electronic / oxidation state
F-CNT	F	685.2	1s	C-F
	C	284.8	1s	C-C/C=C
		286.5	1s	C-O
		287.6	1s	C-F
		290.5	1s	O=C-O
CNT	C	284.8	1s	C-C/C=C
		286.5	1s	C-O
		290.5	1s	O=C-O
Pt/C	Pt	71.71	$4f_{7/2}$	Pt^0
		75.01	$4f_{5/2}$	Pt^0
		72.88	$4f_{7/2}$	Pt^{2+}
		77.70	$4f_{5/2}$	Pt^{2+}
PtZn/CNT	Pt	71.86	$4f_{7/2}$	Pt^0
		75.15	$4f_{5/2}$	Pt^0
		73.21	$4f_{7/2}$	Pt^{2+}
		76.99	$4f_{5/2}$	Pt^{2+}
	Zn	1022.07	$2p_{1/2}$	Zn^{2+}
		1045.15	$2p_{3/2}$	Zn^{2+}
PtZn i-NPs/F-CNT	Pt	71.77	$4f_{7/2}$	Pt^0
		75.14	$4f_{5/2}$	Pt^0
		72.93	$4f_{7/2}$	Pt^{2+}
		76.68	$4f_{5/2}$	Pt^{2+}
	Zn	1021.91	$2p_{1/2}$	Zn^{2+}
		1044.88	$2p_{3/2}$	Zn^{2+}

Table S2 Table for bader charge of F-C, Pt/C, PtZn/C and PtZn i-NPs/F-C.

Sample name	Elements	Bader charge (eV)
F-C	C	1.71
	F	-1.71
Pt/C	Pt	0.29
	C	-0.29
PtZn/C	Pt	-1.75
	Zn	2.02
	C	-0.27
PtZn i-NPs/F-C	Pt	-1.63
	Zn	2.34
	C	1.03
	F	-1.74

Electrochemical Measurements

The electrochemical surface area (ECSA) of Pt was determined in the catalysts using the following equations, respectively:

$$ECSA = \frac{Q_H}{0.21 \times [Pt]}$$

where the QH (mC) is the charge due to the hydrogen adsorption/desorption in the hydrogen region of the CVs, 0.21 mC cm^{-2} is the electrical charge associated with monolayer adsorption of hydrogen on Pt, and [Pt] is the loading of Pt on the working electrode.

The electron transfer number (*n*) was determined by the Koutechy-Levich (K-L) equation：

$$\frac{1}{J} = \frac{1}{J_L} + \frac{1}{j_k} = \frac{1}{B\omega^{1/2}} + \frac{1}{J_k}$$

where J, J_k, and J_L is the measured current density, kinetic current density, and diffusion limited current density, respectively, and the ω is electrode rotation rate, and B is calculated from the slope of the K-L plots:

$$B = 0.62nFC_0(D_0)^{2/3}\nu^{-1/6}$$

Where F is the Faraday's constant (F = 96,485 C mol^{-1}), C_0 is the saturated concentration of O_2 ($C_0 = 1.2 \times 10^{-3}$ mol L^{-1}), D_0 is the diffusion coefficient of O_2 ($D_0 = 1.9 \times 10^{-5}$ cm^2 s^{-1} for 0.1 M $HClO_4$ solution) and ν is the kinetic viscosity of the electrolyte (ν = 0.01 cm^2 s^{-1} for 0.1 M $HClO_4$ solution and).

Four-electron selectivities of catalysts were evaluated on the basis of the electron transfer number (n) and H_2O_2 yield, which were calculated using the following equations:

$$n = \frac{4I_d}{I_d + (I_d/N)}$$

$$H_2O_2\% = 200\frac{I_r/N}{I_d + (I_r/N)}$$

Where I_D and I_R are the Faradaic current at the disk and the ring, respectively; N is the H_2O_2 collection efficiency of the RRDE.